Spinodal Decomposition in a Hydrogen-Bonded Polymer Blend

Manjun He, Yongming Liu, and Yi Feng

Department of Polymer Science and Engineering, East China University of Chemical Technology, Shanghai 200237, People's Republic of China

Ming Jiang

Institute of Materials Science, Fudan University, Shanghai 200433, People's Republic of China

Charles C. Han*

Polymers Division, National Institute of Standards and Technology, Gaithersburg, Maryland 20899

Received May 15, 1990; Revised Manuscript Received July 5, 1990

ABSTRACT: The spinodal decomposition of a hydrogen-bonded binary blend, which consists of a polystyrene with 1.5 mol % of p-(1,1,1,3,3,3-hexafluoro-2-hydroxyisopropyl)-α-methylstyrene comonomer and a poly(butyl methacrylate), has been studied. This system has a LCST with a very asymmetrical phase diagram. Also the critical point does not coincide with the temperature minimum of either the spinodal or the cloud-point curve. The kinetics follows the Cahn–Hilliard–Cook model for early spinodal decomposition and a self-similar mechanism for late-stage coarsening for most cases. For shallow quench cases and for close to glass transition temperature cases, double peaks have been observed during spinodal decomposition, which suggests that a second or an alternative relaxation mechanism may be dominating the coarsening process. A special procedure has been developed to measure the cloud point for this system, which should be applicable to any polymer blend system that has a cloud temperature close to the glass transition temperature.

I. Introduction

The importance of polymer blends is evidenced by not only their ubiquitous presence in commercial products in recent years but also by the fact that they prove to be ideal systems for fundamental studies of phase-separation phenomena.[1] The problem of the very small entropy of mixing for long-chain polymers, which causes most homopolymer blends to be immiscible, has been addressed by many research groups recently. Some promising directions that could enhance the miscibility of polymer blends have been developed, such as (a) chemical grafting,[2] cross-linking,[3,4] and copolymerization,[5-8] (b) introduction of specific interactions like ionic pairs,[9] electron donor/acceptor pairs,[10] and hydrogen-bonded pairs,[11] and (c) flow-induced miscibility.[12,13]

The technique of introducing hydrogen bonding between unlike polymer pairs through chemical modification seems to be a very effective method of producing miscible blends from otherwise immiscible pairs. But the details of the statics and kinetics of phase separation for these hydrogen-bonded systems remain largely unexplored. Painter et al.[14] have developed a theoretical model for associating polymer pairs, and they have also compared their model quantitatively with infrared (IR) and thermal analysis results of several systems. Pearce et al.[11] have made extensive studies by infrared and thermal analysis on a variety of hydrogen-bonded pairs. Cao, Jiang, and Yu[15] have made some IR and morphological studies on hydrogen-bonded systems of a p-(hexafluorohydroxyisopropyl)-styrene containing polystyrene with poly(methyl methacrylate) and poly(butyl acrylate).

In this study, a binary blend of polystyrene which contains 1.5 mol % of p-(1,1,1,3,3,3-hexafluoro-2-hydroxyisopropyl)-α-methylstyrene unit and poly(butyl methacrylate) is used. The purpose of selecting this comonomer at low volume ratio (1.5 mol %) is to minimize the possibility of hydrogen bonding between the same OH-containing monomers[11,15] through dilution effect and to use the low ceiling temperature characteristics of α-methylstyrene to randomly position this OH-containing monomer on the polystyrene chain.[16] The kinetics of phase separation was studied by the temperature-jump light-scattering (TJLS)[17-19] technique, where time-resolved static structure factors were studied. The rate of spinodal decomposition, $R(q)$, is analyzed according to the Cahn–Hilliard–Cook[20,21] theory in the early stages of phase decomposition, and then the extrapolated apparent diffusion coefficients, D_{app}, were used to obtain the spinodal temperature. In the late stage of coarsening, the time dependence of the intensity maximum, I_m, and the corresponding scattering wavevector, q_m, were analyzed by power law dependence.[22,23] Because the phase-separation temperature is not much above the glass transition temperature (~30 °C above T_g), it is very difficult to obtain the cloud-point temperature correctly by conventional scanning rate extrapolation of the onset of scattering intensity increase. Using this technique led to a molecular weight dependence of the cloud point opposite to what one would have expected. Therefore, special attention has been devoted in this study to obtain the true cloud point and metastable gap through reverse quench and melting of phase-separated structures.

In some cases, double-intensity peaks have been observed during spinodal decomposition. For the larger size (lower q) peak, the intensity is growing while the peak position is stationary; this is probably caused by a second relaxation mechanism, similar to the stress relaxation that has been found in metal oxide systems.[24] Although, we cannot rule out the possibilities that this is caused by the possible local inhomogeneity in the starting one-phase system, which is beyond the size range detectable by light scattering, or maybe the system cannot be treated as a simple binary system.

We will briefly discuss the sample preparation in section II, the experimental results and discussion in section III, and finally the conclusion in section IV.

* To whom correspondence should be addressed.

0024-9297/91/2224-0464$02.50/0

II. Sample Preparation

One of the two components used in this binary blend study is a modified polystyrene which contains 1.5 mol % of p-(1,1,1,3,3,3-hexafluoro-2-hydroxyisopropyl)-α-methylstyrene (HFMS) comonomers as shown below and will be abbreviated as PS(OH).

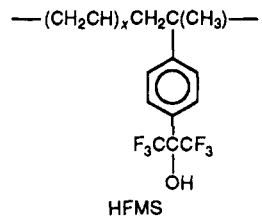

The synthesis procedure is similar to that by Pearce et al.[11] and has been described elsewhere.[15] The purpose in choosing this hexafluoro-2-hydroxyisopropyl group is to minimize the possibility of hydrogen bonding between HFMS groups from the same or different PS(OH) chains through the dilution effect since only a few mole percent of this monomer is enough to change the phase behavior completely.[11,15] Also α-methylstyrene is chosen for its low-ceiling temperature in order to eliminate possible HFMS sequences for a more random distribution.[16] The radically polymerized PS(OH) was purified in CH_2Cl_2/petroleum ether. The molecular weight of 3.7×10^4 and molecular weight distribution of $M_w/M_n = 1.7$ was measured by GPC. The comonomer HFMS concentration is determined by the monomer ratio of the feed for copolymerization. The second component of the blend, poly(butyl methacrylate) (PBMA), is also radically polymerized and then fractionated in CH_2Cl_2/CH_3OH with $M_w = 4.2 \times 10^4$ and $M_w/M_n = 1.5$.

Specimens of PS(OH)/PBMA at different compositions were prepared by casting from benzene solutions (~10% total polymer concentration) of desired polymer compositions on glass surfaces for DSC measurements and on quartz window plates for temperature-jump light-scattering measurements. All specimens are dried in a vacuum oven at 70 °C for at least 7 days before measurements.

Differential scanning calorimetry (DSC) runs were carried out on a Perkin-Elmer[25] instrument at a heating rate of 10 °C/min. The temperature-jump light-scattering (TJLS) measurements were carried out on a time-resolved static light-scattering instrument,[19] which uses a 5-mW He–Ne laser as the light source and a set of lenses for scattering light collection, collimation, and angular mapping onto a linear photodiode array detector (Radicon tube). An optical multichannel analyzer (OMA3) is used for data acquisition. Collimation and scattering sample size desmearing is carried out in the optical field by the lens system.

Two sets of heating blocks were used for the temperature-jump experiments: One was used to preheat the sample to a temperature below the binodal temperature in the miscible region while the other was controlled at a desired experimental temperature. Temperatures are controlled by PID controllers to within 0.02 °C of specified temperatures. It takes about 1 min to reach temperature equilibrium after transfer of the sample cell from one heating block to the other for a temperature-jump; therefore, the initial time of the experiment is chosen to be at the end of 1 min after transferring the sample. The sensitivity of the radicon detector was calibrated by fluorescence radiation from Nile Blue dye (5×10^{-6} g/mL) embedded in gelatin gel in a flat cell of 100-μm thickness.

III. Results and Discussion

The PS(OH)/PBMA blends casted from benzene solutions exhibit a pronounced single glass transition temperature in all compositions. The DSC runs for PS(OH) and blends at 30.9, 41.5, 55.4, and 70.4 wt % of PBMA are shown in Figure 1a. The 85.0 wt % and pure PBMA samples were run at lower temperatures and therefore were not displayed in Figure 1a. The glass transition temperatures obtained from the midpoint as indicated in Figure 1a are plotted in Figure 1b. This DSC study clearly demonstrated that all solution-casted samples are miscible.

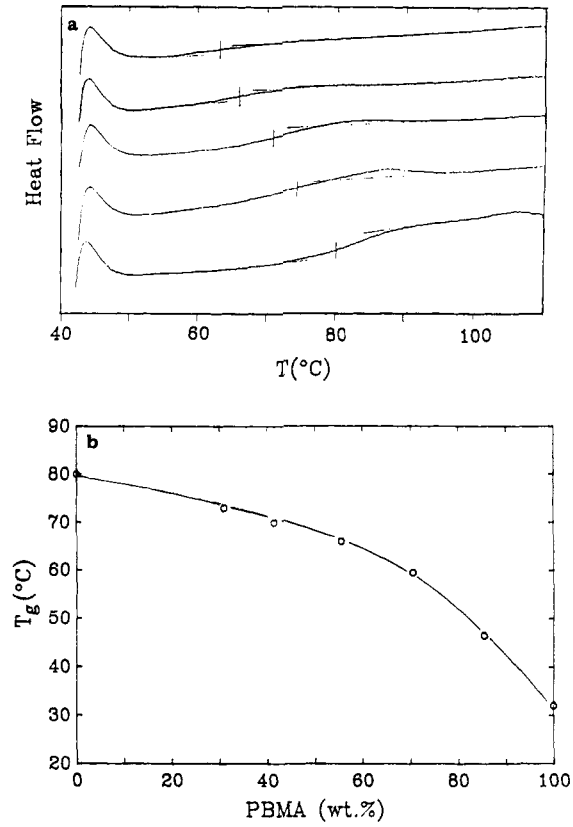

Figure 1. (a) Differential scanning calorimetry runs for PS(OH)/PBMA samples. From top to bottom with PBMA composition at 70.4, 55.4, 41.5, 30.9, and 0 wt %, respectively. The glass transition temperatures are obtained from the midpoint as indicated by the pips. (b) Glass transition temperatures obtained from Figure 1a together with two-additional ones at 85.0 wt % and pure PBMA. The solid curve is arbitrarily drawn to follow the points.

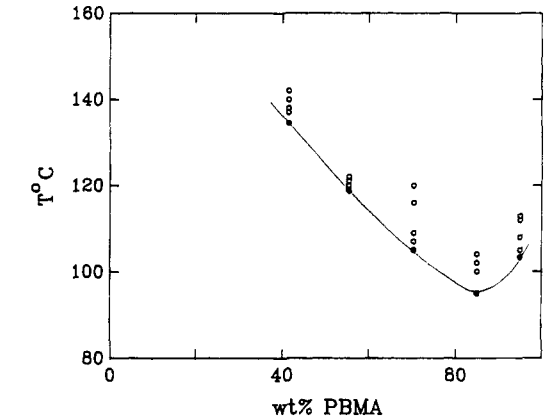

Figure 2. Spinodal temperatures obtained by extrapolating the D_{app}'s to zero at various compositions shown as filled circles together with all the temperatures (shown as open circles) where temperature-jump measurements have been carried out. The solid curve is the spinodal line arbitrarily drawn through all experimental points.

Attempts to obtain the cloud-point curve by conventional techniques, i.e., using a single-point scattering detector to monitor the onset of an abrupt increase of scattering intensity as the sample was heated at a constant rate, led to an erroneous reverse molecular weight dependence of LCST cloud-point curves. The larger molecular weight blends, which have a very small mobility partly due to the phase-separation temperature being not

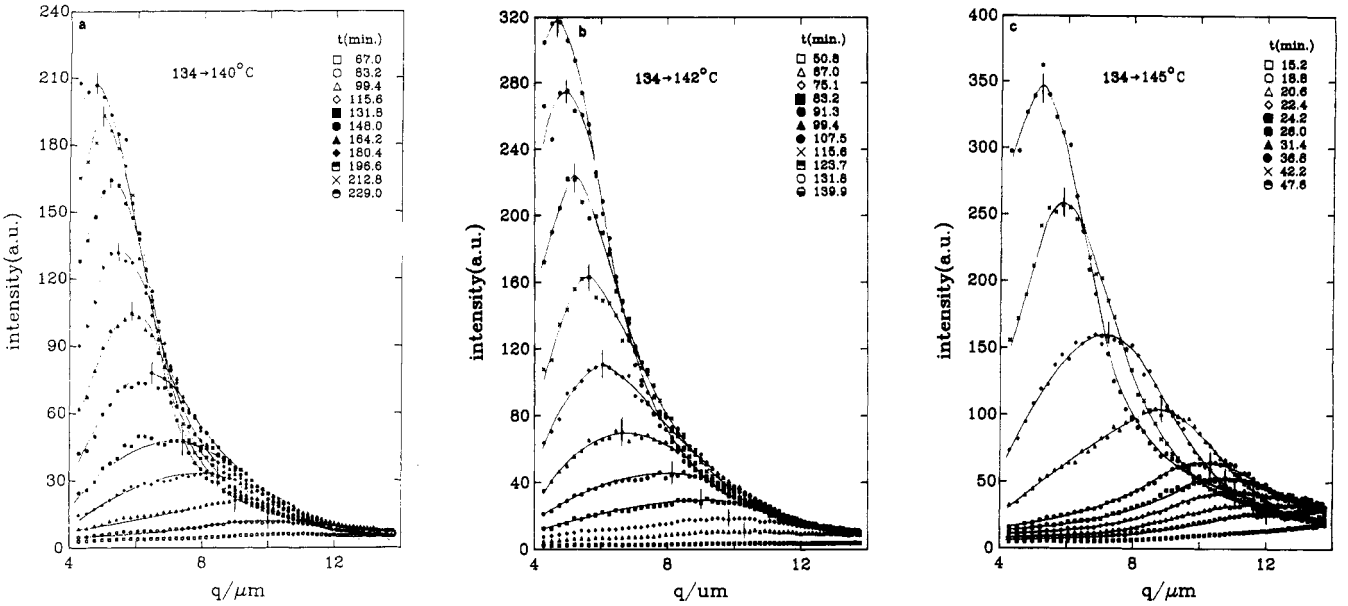

Figure 3. Scattering intensities versus q for a 41.5 wt % PBMA sample at various times as indicated on the graphs after jumped into spinodal region: (a) jump from 134 to 140 °C, (b) jump from 134 to 142 °C, (c) jump from 134 to 145 °C.

much above the glass transition temperature, extrapolate to zero heating rate to give an apparently higher cloud point than the lower molecular weight blends. Similar behavior has been observed in polystyrene/poly(*p*-chlorostyrene) blends.[26] Therefore, a much more tedious procedure has been used and will be discussed later to obtain the cloud-point curve.

The temperature-jump light-scattering technique[19] is used to study the spinodal decomposition of these PS(OH)/PBMA blends at various compositions and jump (quench) depths as indicated by open circles in Figure 2. The scattering intensity, $I(q,t)$, which is proportional to the static structure factor, $S(q,t)$, at different times after the jump into the spinodal region, is recorded and stored by an optical multichannel analyzer. For example, the scattering intensity, $I(q)$, for a 41.5% blend jumped from 134 to 140 °C is plotted against the scattering wavevector, q, for different times as indicated in the graph of Figure 3a. Similarly plots for the sample jumped from 134 to 142 and 145 °C are displayed in parts b and c of Figure 3, respectively. We should point out that only a few of the time frames actually collected are displayed in parts a–c of Figure 3 to demonstrate the typical qualitative features of the spinodal ring development and coarsening. The early-stage data for the 41.5% sample jumped from 134 to 140 °C are plotted as ln $I(q)$ versus time for different q in Figure 4a. Also, a similar plot for the 55.4% sample jumped from 90 to 122 °C is displayed in Figure 4b. It should be noted that the longest time in these plots is 800 s, which is much earlier than the first curve of 67 min plotted in Figure 3a.

According to Cahn–Hilliard–Cook theory[20,21] the scattering intensity in the early stage of spinodal decomposition can be written as

$$I(q,t) = I_\infty(q) + [I_0(q) - I_\infty(q)]e^{2R(q)t} \quad (1)$$

where $I_0(q)$ and $I_\infty(q)$ are related to the initial structure factor and the final "virtual" structure factor as discussed in previous papers.[18,19] The growth rate

$$R(q) = -Mq^2\left[\frac{\partial^2 f}{\partial \phi_0^2} + 2\kappa q^2\right] \quad (2a)$$

$$R(q) = -D_{app} = q^2 - 2M\kappa q^4 \quad (2b)$$

with M the mobility, $\partial^2 f/\partial \phi_0^2$ the second derivative of free energy of mixing with respect to composition at initial composition ϕ_0, and κ the interfacial free energy density. Again, q is the scattering wavevector with $q \equiv (4\pi/\lambda)\sin\theta/2$, where λ is the wavelength of the incident radiation in the medium and θ is the scattering angle.

If one can detect enough scattering intensity in the early stage of spinodal decomposition, then it is possible to use a $^1/_3$ power plot as discussed in eq 15 of ref 19 to obtain good extrapolated values of $R(t)$. But in the case where the scattering intensity is weak in the early stage as is the case in this PS(OH)/PBMA study, it is very difficult to carry out an interactive plot (with experimental data on both sides of the equation) as used in ref 19. Therefore, we have decided to use the semilogarithmic plot of ln $I(q,t)$ versus t as shown in Figure 4 to obtain $R(q)$. The virtual structure factor, $I_\infty(q)$, is assumed to be negligible in this procedure. This may not be a bad assumption in most cases,[17] since $I_\infty(q)$ is only significant when the quenched temperature is very close to the critical temperature and also the time is very early.[18] $R(q)$ values obtained from this procedure for the 41.5% PBMA sample are plotted as $R(q)/q^2$ versus q^2 for different quench depth as shown in Figure 5. The intercept from the linear extrapolation gives the apparent diffusion coefficient, D_{app}, according to eq 2b. Since the spinodal temperature is where D_{app} becomes zero (because $\partial^2 f/\partial \phi^2 = 0$), therefore, $-D_{app}$ values obtained above are plotted against T as shown in Figure 6 for this 41.5% sample in order to find the spinodal temperature. The spinodal temperature, T_s, thus obtained from the extrapolation is 134.5 °C. Similar procedures have been carried out for 41.5%, 55.4%, 70.4%, 85.0%, and 95.0% samples, and the corresponding spinodal temperatures are plotted as filled circles in Figure 2.

From the scattering peak positions and peak intensities shown in parts a–c of Figure 3, the late-stage coarsening of the structure on the power law dependence of time can be studied.[22,23] If we pick off the peak position and intensity as shown by the vertical pips in parts a–c of Figure 3, as a function of time, then we can plot the intensity maximum and the q position of the maxima as a function of time in a log–log scale as shown in parts a and b of Figure 7, respectively. The solid lines in Figure 7a were drawn with slope 3 and in Figure 7b with slope −1. These

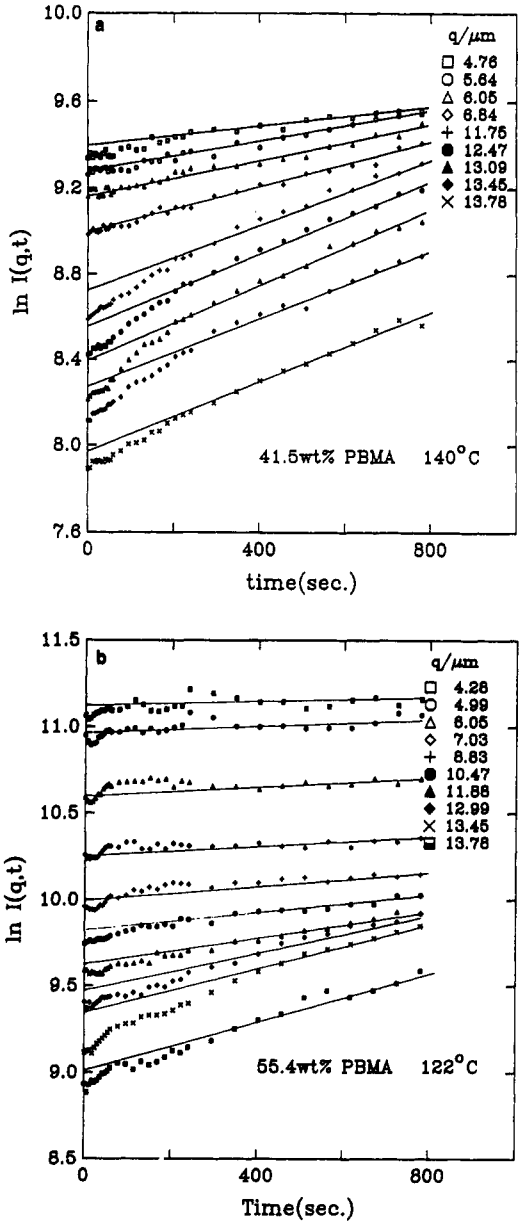

Figure 4. Semilogarithmic plot of scattering intensities versus time at early stages after jump into spinodal region for different q values as indicated in the graph: (a) for 41.5 wt % PBMA sample jump from 134 to 140 °C and (b) for 55.4 wt % of PBMA sample jump from 90 to 122 °C.

slopes imply a coarsening mechanism of a self-similar structure suggested by Siggia.[23] Indeed, the structure factor during these coarsening periods can be scaled together as shown in parts a and b of Figure 8, with $X = q/q_m$ and $F(X) = I(q)\,q_m^3$. The solid line is the structure factor proposed by Furukawa[22] for a cocontinuous self-similar structure from spinodal decomposition of a binary mixture with critical composition, which can be expressed as

$$F(X) = X^2/(3 + X^8) \tag{3}$$

The smaller coarsening rate in the intermediate stage can be seen from the deviation from slope = −1 in Figure 7b for a quench temperature of 139 and 140 °C. Also the deviation at very late time of the 140 °C data in Figure 7b may be caused by the later stage slowing down after the cocontinuous structure has broken up. Although the scattering structure factors do not scale perfectly as shown in parts a and b of Figure 8, but in general, they do scale

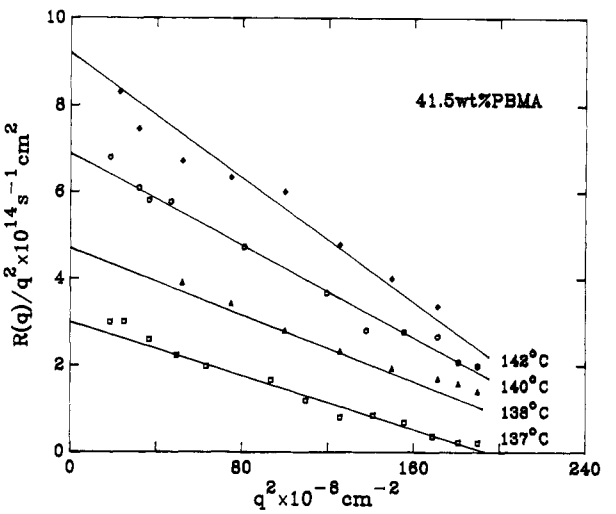

Figure 5. Rate of growth, $R(q)$'s, obtained from ln $I(q,t)$ vs t plots displayed as $R(q)/q^2$ vs q^2 for the 41.5 wt % PBMA sample at various final temperatures as shown in the graph. The straight lines fitted to the data points according to eq 2 are used to obtain D_{app}'s from the intercepts.

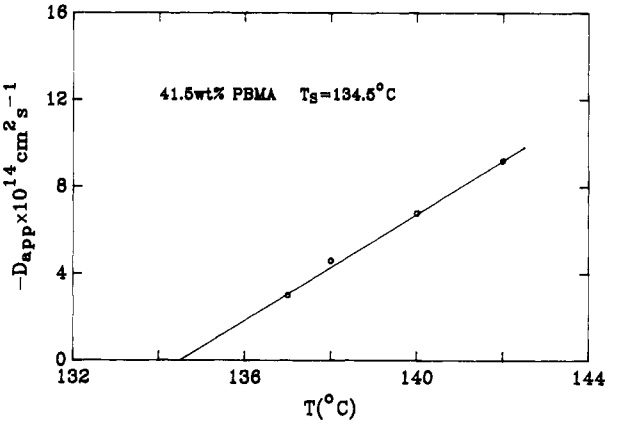

Figure 6. D_{app}'s obtained from Figure 5 plotted as $-D_{app}$ vs T. The extrapolated temperature at $D_{app} = 0$ is the spinodal temperature. For this 41.5 wt % PBMA sample, the extrapolated spinodal temperature is 134.5 °C.

into a universal functional form and can be represented well by the Furukawa structure factor.

It should be pointed out that the Furukawa functional form we have used in these plots is the functional form for the critical composition. There is no way we can match the scaled experimental structure factor to the off-critical function form of

$$F(X) = X^2/(2 + X^6) \tag{4}$$

The question of whether 41.5% PBMA is close to the critical composition or not becomes an interesting one. On the other hand, the spinodal curve as shown in Figure 2 has an asymmetrical shape with the minimum at around 85% of PBMA concentration. The asymmetrical phase diagram normally occurs in binary systems either with a very different molecular weight ratio[27] or with a strong composition-dependent interaction parameter, χ.[28] The molecular weights of PS(OH) and PBMA are similar in this study; therefore, the asymmetrical spinodal line is most probably caused by the strong interaction of hydrogen bonding. If we count the possible number of interaction sites of PS(OH) and PBMA, it is obvious that the ratio is very different from one. This is because only 1.5 mol % of styrene monomers are replaced by the ones that contain an OH group. In other words, there are on the

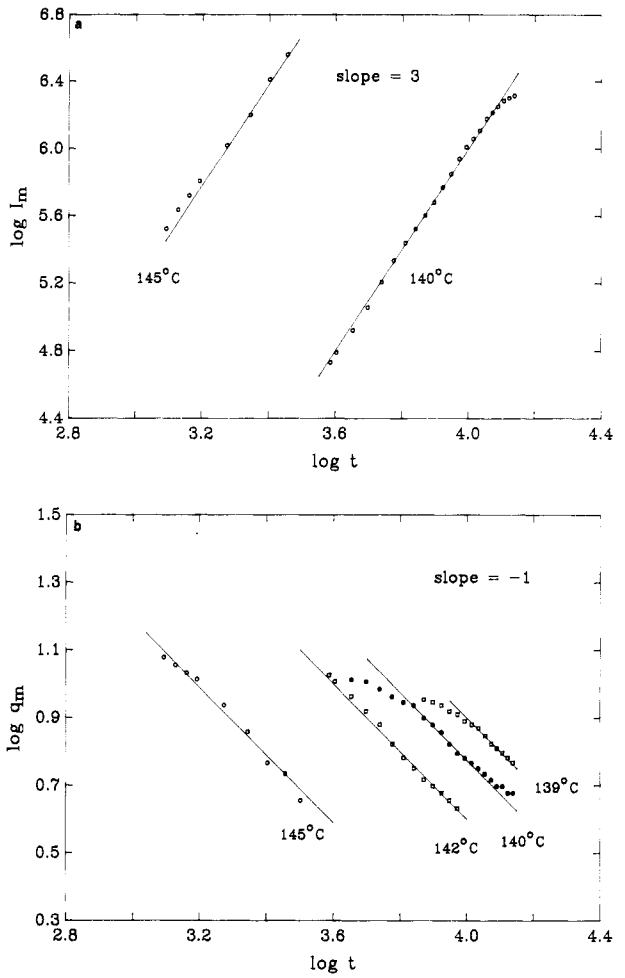

Figure 7. (a) Scattering intensity maximums in the late stage after jumped into spinodal region for the 41.5 wt % PBMA sample obtained from Figure 3 plotted as log I_m vs log t for 140 and 145 °C. Slope = 3 lines are also plotted to show the power law dependence of the intensity growth. (b) Corresponding q-positions for the intensity maximum, q_m, plotted as log q_m vs log t. Slope = −1 lines are drawn to show the power law dependence of the q_m change.

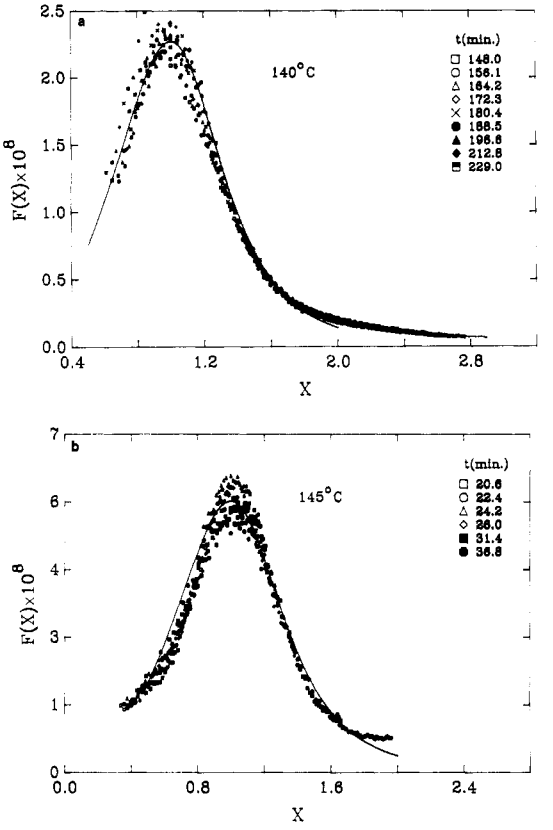

Figure 8. Scaled intensities $F(X) = I(q,t)\ q_m^3$ plotted against reduced wavenumber $X = q/q_m$ for various times after jumped into spinodal region for the 41.5 wt % PBMA sample. The solid line is the Furukawa scattering structure factor of eq 3 for critical composition: (a) jumped from 134 to 140 °C and (b) jumped from 134 to 145 °C.

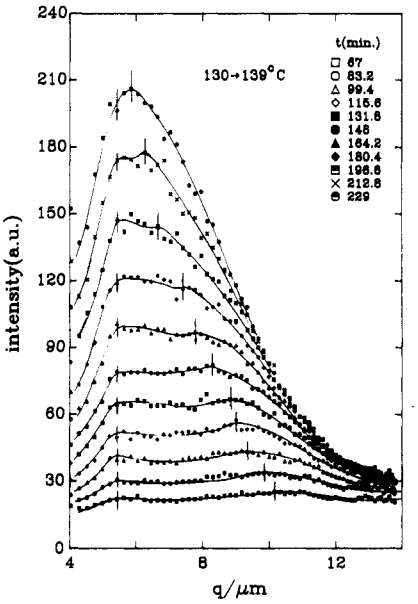

Figure 9. Scattering intensities versus q for a 41.5 wt % PBMA sample at various times as indicated on the graph, after jumped from 130 to 139 °C.

average only 6 OH-containing monomers/each polystyrene chain compared to 300 carbonyl groups/each PBMA chain that are available to form interaction pairs. If we replace the number of monomer units by the number of interaction sites, then the lattice theory should predict an asymmetric phase diagram with the critical point (also the minimum) at a low concentration of PBMA. This is opposite to what is observed experimentally. In addition, the critical temperature (which will be discussed later) does not correspond to the minimum of the spinodal curve, which can only be explained by a compositional dependence of enthalpic interaction and polydispersity in distribution. A quantitative explanation can only be obtained from the exact temperature and composition dependence of the free energy function which may be obtained by small-angle neutron scattering.[28] Although, we should point out that the spinodal curve of a poly(butyl methacrylate)/poly(styrene-*co*-vinylphenol) blend has been calculated by Serman et al.[29] with an association model. Features of LCST and the asymmetrical spinodal curve reported are very similar to the experimental results shown in this paper.

The question of the distribution of the number of HFMS monomers on different polystyrene chains may be very important considering the small number (average of 6) of HFMS monomers per polystyrene chain. The fraction of PS chains that contain no OH group is small, about 0.24% ($(1 - 6/N)^N$, with N = degree of polymerization); nevertheless, this is not zero. Whether this PS(OH)/PBMA system has to be treated as a multicomponent system or can be approximated as a pseudo binary system with polydispersity is unknown. An unusual phenomenon we have observed in this kinetics study is the observation of double peaks in the relatively late stage of a shallow quenched 41.5% blend and also for the 70.4% blend as

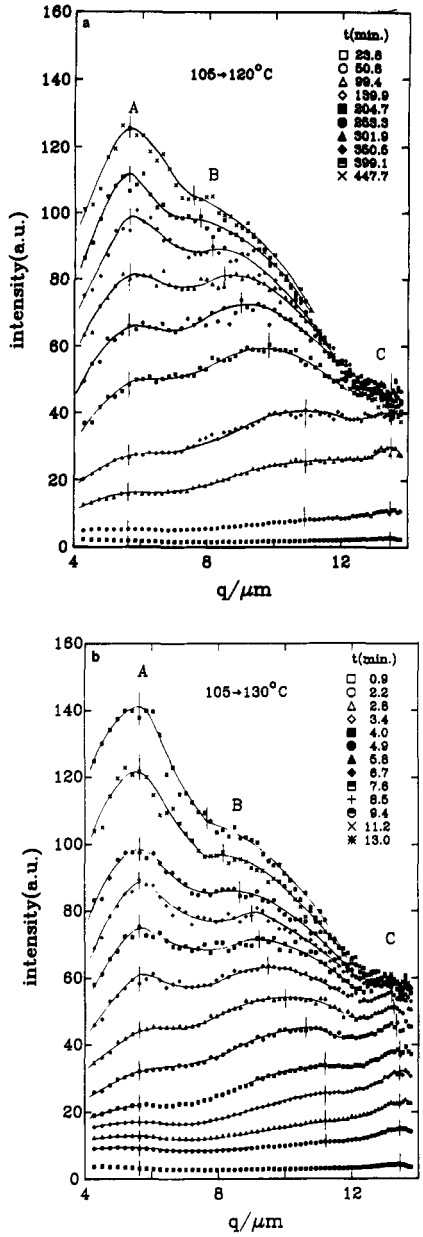

Figure 10. Scattering intensities versus q for a 70.4 wt % PBMA sample at various times as indicated on the graph: (a) jumped from 105 to 120 °C and (b) jumped from 105 to 130 °C.

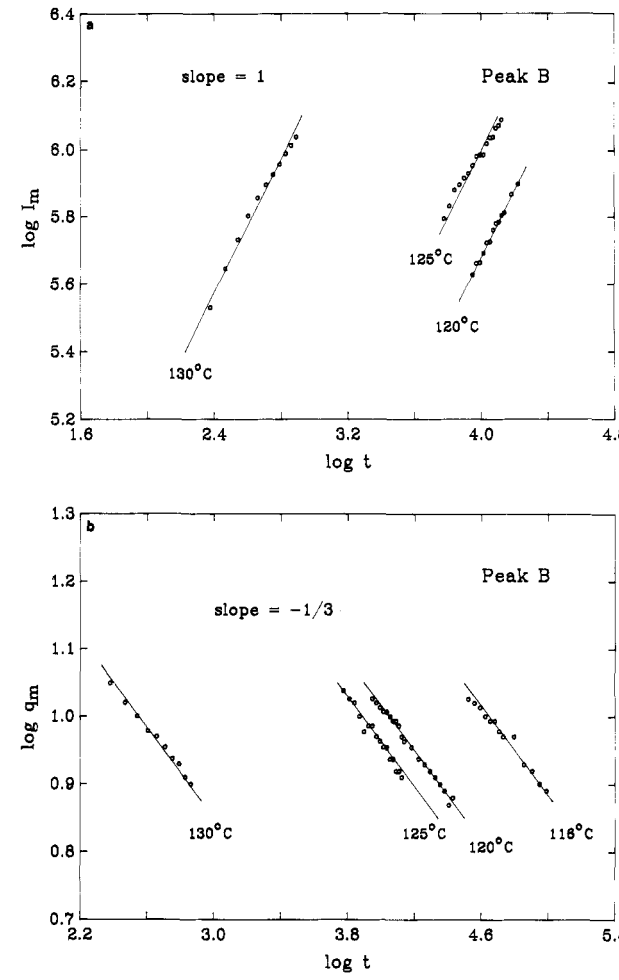

Figure 11. (a) Intensity maximums for the peak B of the 70.4 wt % PBMA sample after jumped into spinodal region plotted as log I_m versus log t for the temperature of 120, 125, and 130 °C as indicated on the graph. Slope = 1 lines are also plotted to show the power law dependence of the intensity growth. (b) Corresponding q-positions for the intensity maximum, q_m, plotted as log q_m vs log t. Slope = $-1/3$ lines are plotted to show the power law dependence of the q_m change.

shown in Figure 9 and parts a and b of Figure 10, respectively. It is clear that the peak at larger q value (peak B) starts to develop first, and then the peak at smaller q value (peak A) starts to grow and becomes dominate. Peak B gradually grows and merges into peak A. The intensity of peak A is growing while the q-position remains constant. If we examine the power law dependence of these I_m's and q_m's, we found that, as plotted in parts a and b of Figure 11, respectively, the I_m's for the 70.4% PBMA sample (peak B) follow a t^1 dependence and the q_m's follow a $t^{-1/3}$ dependence. Similar power law dependences for the shallow quenched (from 130 to 139 °C) 41.5% sample have also been observed. However, at the same time scale, the peak A remains stationary (constant q_m) while the peak intensity follows an exponential growth first and then switches over to a power law growth. This can be seen in Figure 12, where the peak A intensities from Figure 10a are plotted versus time in semilogarithmic scale in Figure 12a and logarithmic scale in Figure 12b. The growth of intensity is exponential or linear in a semilogarithmic plot for the first 3000 s as shown in Figure 12a and then switches over to a power law growth (linear in log–log plot) as shown in Figure 12b. The slope of Figure 12b is approximately 1.6. The same behavior can be observed for other cases. The results of Figure 10b are plotted in parts a and b of Figure 13. The power in the power law growth region is approximately 1.7. Slowing down from power law growth is also observed after about 16 000 s in Figure 12b and after 500 s in Figure 13b.

Although the power in the power law growth region and the stationary peak position of peak A cannot be explained by simple linear[20,21] or nonlinear[22,23,30] theories, these phenomena strongly suggest that another mechanism may exist that controls the fluctuation growth at a larger scale, which has not been observed for non-hydrogen-bonded binary systems (for example, polystyrene/poly(vinyl methyl ether)[17-19]). In the polystyrene/poly(vinyl methyl ether) case, spinodal temperatures are also much higher than the glass transition temperature of the blend and of both phase-separated components. However, it has been suggested by Stephenson[24,31] that, if one of the network-forming components has a very high viscosity, then a rate-limiting process can be switched from the diffusion of the more mobile component to the stress relaxation of the less mobile component via a mechanism of network dilation by viscous flow. Stephenson's model does not offer double growth peaks, because the second rate-limiting process is

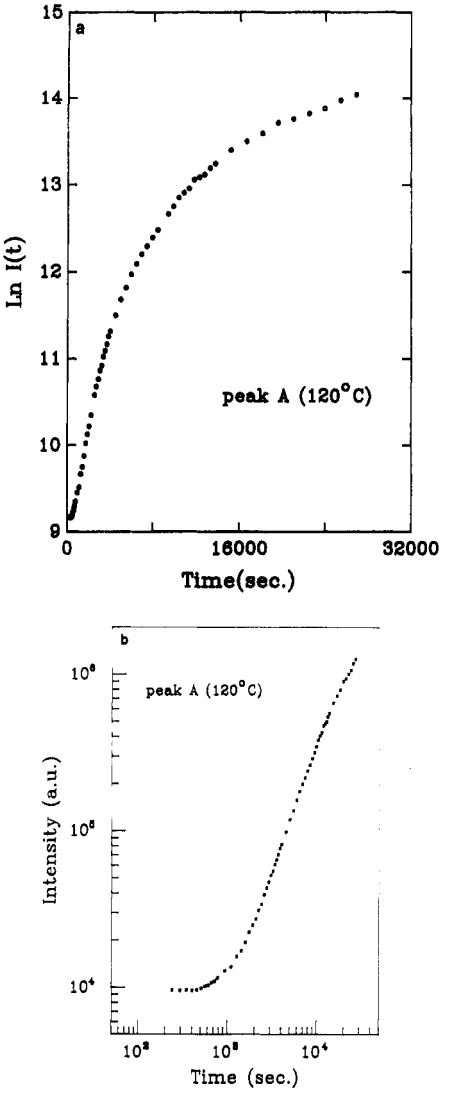

Figure 12. Intensity maximums for the peak A of the 70.4 wt % PBMA sample after jumped from 105 to 120 °C plotted in (a) as ln $I(t)$ vs t to show the initial exponential (linear in this plot) growth for time shorter than 3000 and (b) as log $I(t)$ vs log t to show the switchover to a power law growth (linear in this plot) for time from 3000 to 10^4 s.

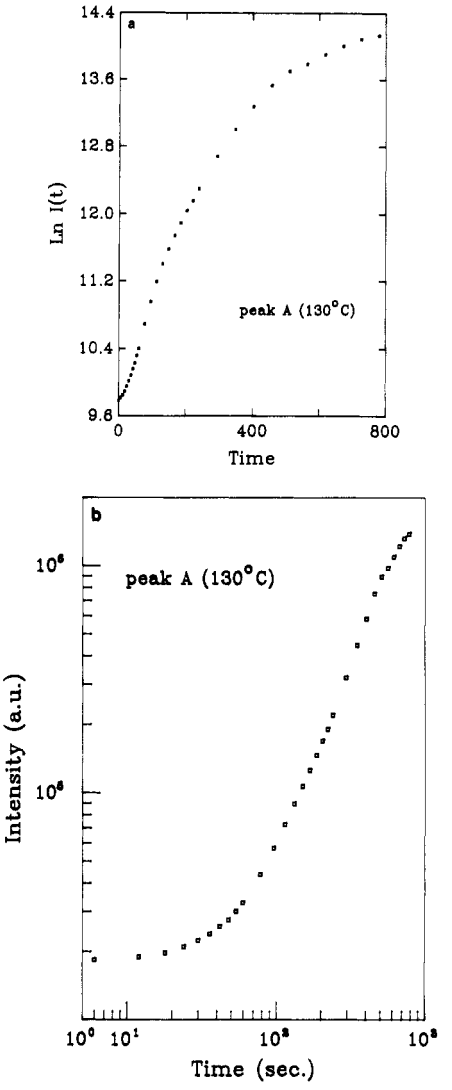

Figure 13. Same sample as in Figure 12 after jumped from 105 to 130 °C plotted (a) as ln $I(t)$ vs t to show the initial exponential growth for time shorter than 150 s and (b) as log $I(t)$ vs log t to show the switchover to a power law growth for time from 150 to 500 s.

a relaxation process (instead of a diffusional process) that does not have the usual q^2 dependence term[31] as in the CHC theory. But it is still possible that a second mechanism exists in the PS(OH)/PBMA case; the rate-limiting process could have changed once the network started to form.

If one of the network-forming components (e.g., the PS-(OH)-rich component) has a much smaller mobility because it is closer to its T_g or because it has much higher number of hyrogen bonds, then the growth of this network could become the rate-limiting process. As long as the dimension of this network component has not changed, the q_m will be stationary in the scattering experiment. Although this mechanism may be plausible, it is just speculation at this time. More detailed theoretical and experimental studies are necessary in order to elucidate this phenomena. Also, we cannot rule out other possibilities, such as the following: (i) multiple peaks may be caused by simultaneous phase separation of the system into multiple components and the polydispersed PS(OH)/PBMA has to be treated as a multicomponent system; (ii) the possible existence of local inhomogeneity in the starting one-phase material, which is beyond the size range detectable by light scattering but can alter the initial state or states of the spinodal decomposition process. In Figure 14, we have tried to scale the scattering structure factors of the 70.4% PBMA sample from Figure 10b according to the q_m of peak B. It is clear that all peak B's can be scaled together reasonably well considering the large overlap between peaks A and B. We have also plotted the Furukawa structure factor for the off-critical composition (eq 4) as the solid line in Figure 14a, but in this case the shape is not matched. We did not include the critical structure factor (eq 3); since it has a peak narrower than the off-critical one, there is no chance to match it with experimental results. The falling edge of peak B has a slope close to −2 as shown in Figure 14b, which is much smaller (in absolute value) than the −4 required for the scattering of flat interfaces observed by Hashimoto et al.[32] in the large q region. Besides the independent growth of peak B discussed earlier, this slow decrease in intensity at large q also demonstrates that this peak cannot be explained as the crossover from self-similar structure to interfacial scatteing as q increases as observed by Hashimoto et al. Also, it is clear from parts a and b of Figures 10 and 14 that even higher order peaks exist. The origin and interrelationship among these peaks are not clear at this time.

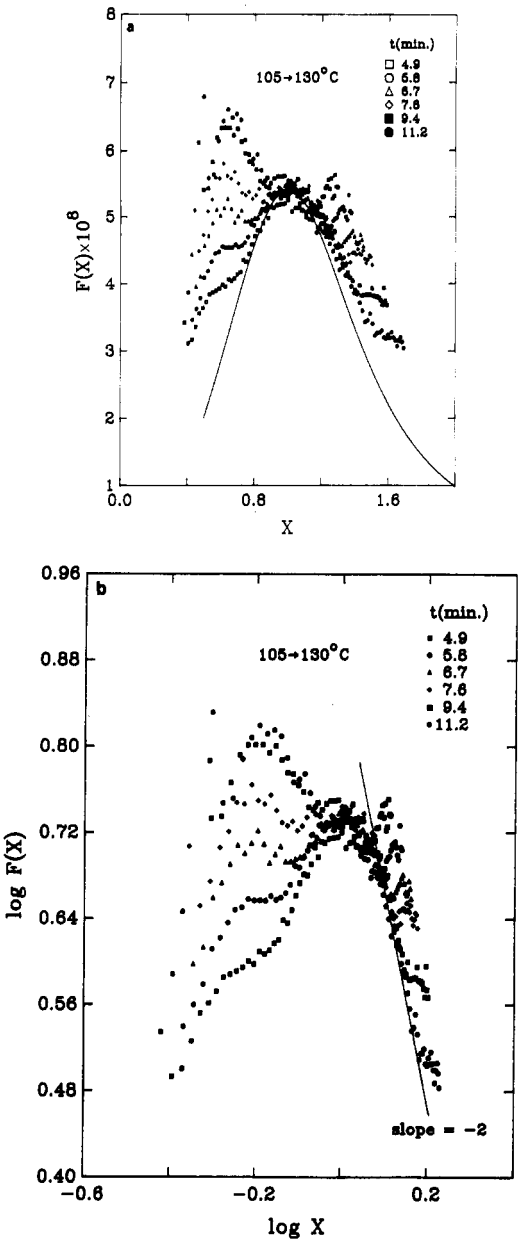

Figure 14. Scaled intensities according to the q_m of peak B plotted against reduced wavenumber for various times after jumped from 105 to 130 °C for the 70.4 wt % PBMA sample: (a) in linear scale together with the Furukawa structure factor of off-critical composition (eq 4) in a solid line and (b) in log–log scale together with a solid straight line with a slope of −2.

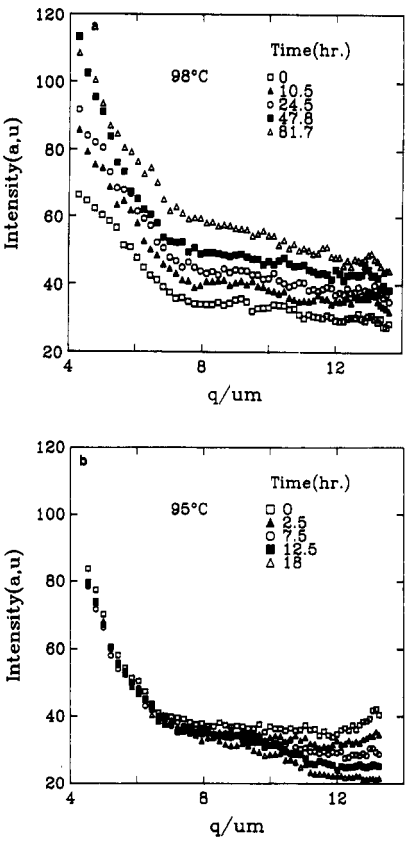

Figure 15. 70.4 wt % PBMA blend sample temperature jumped from 95 to 109 °C for approximately 1 h and (a) quenched back to 98 °C, which is still in the metastable region (The scattering intensity, $S(q)$, is displayed as a function of q for different times after the quench. Continuous growth of $S(q)$ can be observed.) and (b) quenched back to 95 °C, which is in the miscible region. The melting of the structure is indicated from the decrease of $S(q)$ as a function of time.

Table I
Measured Spinodal (T_s) and Cloud (T_c)

compositn (PBMA %)	T_s	T_c
41.5	134.5	134.5
55.4	118.8	
70.4	105	96
85.0	95	87
95.0	103.4	99

Except for the problem of possible switchover of the rate-limiting mechanism at low quench temperatures and high PBMA compositions, the questions of the reversibility, the cloud-point curve, and the behavior in the metastable region for this PS(OH)/PBMA system are also interesting and the possible differences from regular binary polymer blends should be studied. As we have mentioned before, because of the slow growth rate, $R(q)$, it is difficult to measure the cloud-point temperatures correctly. We have found that we can obtain the cloud-point temperature successfully with the following procedure: (i) First we take the blend into the unstable region for a relatively short time (could be 1 h in this case), wait until the structure factor, $S(q)$, starts to grow and (ii) quench the specimen back to a lower temperature, T_1. The structure generated will start to melt away if this temperature, T_1, is in the miscible region, but it will continue to grow if T_1 is still in the metastable region or in the unstable region. For example, in Figure 15a, a 70.4 wt % PBMA blend has been jumped from 95 to 109 °C (inside the unstable region, T_s = 105 °C) for approximately 1 h and quenched back to 98 °C. The scattering intensity, $S(q)$, is displayed as a function of q for different times after quench back to 98 °C. It can be seen that $S(q)$ is still growing at all q's. This indicates that the blend is in the metastable region without a characteristic growth maximum for spinodal growth. However, if we repeat the same procedure but quench back to a lower temperature, such as 95 °C, then the structure factor will show characteristic melting as illustrated by Figure 15b. When this somewhat tedious procedure is repeated, cloud-point temperature can be obtained, which are listed in Table I together with spinodal temperatures obtained earlier. The important part of this procedure is to develop a finite size structure in the unstable region and then use the melting process to determine the cloud point. The advantage of this is to avoid the dependence on the unknown nucleation process and the critical nucleation size, which could mislead the interpretation of a conventional temperature scanning cloud-point measurement.

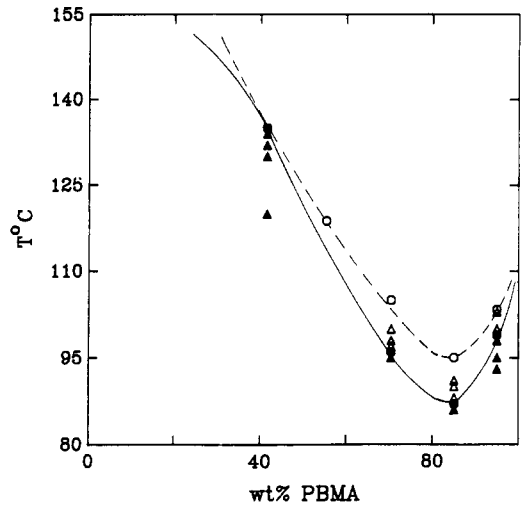

Figure 16. Cloud points shown in filled circles, together with all the temperatures (shown in open triangles) where intensity growth has been observed and temperatures (shown in filled triangles) where melting of the structure from reverse quench has been observed. The solid line is arbitrarily drawn through cloud points. The spinodal line from Figure 2 is also shown as a dotted line, together with spinodal temperatures obtained experimentally as open circles.

The measured cloud points are plotted as filled circles in Figure 16, together with all temperatures where measurements for cloud-point temperature have been carried out. The filled triangles indicate the blend is in the miscible region at that temperature while the open triangles indicate the blend is in the metastable region. The solid line is an arbitrarily drwon cloud-point curve through the data points. The dotted line is the spinodal curve together with the spinodal temperatures obtained earlier as shown in Figure 2. It is clear that the critical point is at about 40% of PBMA composition instead of 85% where the minimum temperatures of both cloud-point and spinodal curves are. This could explain why the 41.5% sample exhibits a self-similar structure indicative of the critical composition during the coarsening process as indicated in Figure 8.

IV. Conclusion

In this study, the equilibrium phase diagram, which includes the cloud-point curve and the spinodal curve, has been obtained for a hydroxy-modified polystyrene/poly(butyl methacrylate) system. The phase-separation kinetics in the unstable region has been studied by the temperature-jump light-scattering technique. The comonomer, HFMS, used in the modification of polystyrene has been found to be very effective in introducing miscibility into this blend system. Certain static and dynamic characteristics of this system are different from a weakly interacting system and will be listed as follows:

1. The phase diagram is very asymmetrical but opposite to the direction that a simple counting of the ratio of interacting pairs will lead to.

2. The critical composition is at about 40 wt % of PBMA, which is very different from the composition corresponding to the minimum temperatures of either the spinodal curve or the cloud-point curve. It is possible that this is caused by the broad distribution[33] of HFMS in different polystryene chains, which includes both number and position distributions.

3. The kinetics follows the CHC model for early spinodal decomposition and a self-similar mechanism for late-stage coarsening for most cases. Double and multiple peaks have been observed during the spinodal decomposition for shallow quenches and close to the glass transition temperature. This indicates the possibility of a second or alternative mechanism involved in the coarsening process.

4. A special procedure, which relies on the melting instead of the growth of the phase-separated structure, has been used successfully in this study to determine cloud-point temperatures. This procedure should be applicable to any blend system, especially for one that has a cloud-point temperature close to its glass transition temperature.

We believe more theoretical as well as experimental studies are needed for these types of hydrogen-bonding systems. It is important to study the free energy function as well as the critical behavior of a strong interacting system such as this PS(OH)/PBMA system. The distribution of hydroxy-carrying comonomer may be very important. Small-angle neutron-scattering experiments are being planned in order to answer some of these questions.

Acknowledgment. We thank Drs. Cathy Jackson and Shu-Shing Chang for their assistance in DSC measurements and Drs. Hongdoo Kim and Robert Briber for their help on computer programming. Stimulating discussion from Dr. Charles Guttman is also acknowledged.

References and Notes

(1) Paul, D. R.; Newman, S., Eds. *Polymer Blends*; Academic Press: New York, 1978; Vols. I and II. Olabisi, O.; Robeson, L. M.; Shaw, M. T. *Polymer–Polymer Miscibility*; Academic Press: New York, 1979.
(2) Paul, D. R.; Sperling, L. H., Eds. *Multicomponent Polymer Materials*; Advances in Chemistry Series 211; American Chemical Society: Washington, DC, 1986.
(3) Bauer, B. J.; Briber, R. M.; Han, C. C. *Macromolecules* **1989**, *22*, 940.
(4) Briber, R. M.; Bauer, B. J. *Macromolecules* **1988**, *11*, 3296.
(5) ten Brinke, G.; Karasz, F. E.; MacKnight, W. J. *Macromolecules* **1983**, *16*, 1827.
(6) Kamboar, R. P.; Bendler, J. T.; Bopp, R. C. *Macromolecules* **1983**, *16*, 753.
(7) Paul, D. R.; Barlow, J. W. *Polymer* **1984**, *25*, 487.
(8) Sakurai, S.; Hasegawa, H.; Hashimoto, T.; Hargis, I. G.; Aggarwal, I. G.; Han, C. C. *Macromolecules* **1990**, *23*, 451.
(9) E.g.: Simmons, A.; Eisenberg, A. *Polym. Prepr. (Am. Chem. Soc., Div. Polym. Chem.)* **1986**, *27* (1), 341.
(10) E.g.: Rodriguez-Parada, J. M.; Percec, V. *Macromolecules* **1986**, *19*, 55.
(11) Pearce, E. M.; Kwei, T. K.; Min, B. Y. *J. Macromol. Sci., Chem.* **1984**, *A21*, 1181.
(12) Hashimoto, T.; Takebe, T.; Suehiro, S. *J. Chem. Phys.* **1988**, *88*, 5874. Takebe, T.; Sawaoka, R.; Hashimoto, T. *J. Chem. Phys.* **1989**, *91*, 4369.
(13) Nakatani, A. I.; Kim, H.; Takahashi, Y.; Han, C. C. *Polym. Commun.* **1989**, *30*, 143. Nakatani, A. I.; Kim H.; Takahashi, Y.; Matsushita, Y.; Takano, A.; Bauer, B. J.; Han, C. C., submitted for publication in *J. Chem. Phys.*
(14) Painter, P. C.; Park, Y.; Coleman, M. M. *Macromolecules* **1989**, *22*, 570. Painter, P. C.; Park, Y.; Coleman, M. M. *Macromolecules* **1989**, *22*, 580. Coleman, M. M.; Lichkus, A. M.; Painter, P. C. *Macromolecules* **1989**, *22*, 586.
(15) Cao, X.; Jiang, M.; Yu, T. *Makromol. Chem.* **1989**, *190*, 117.
(16) Odian, G. *Principles of Polymerization*, 2nd ed.; John Wiley and Sons: New York, 1981; Chapter 2.
(17) Kumaki, J.; Hashimoto, T. *Macromolecules* **1986**, *19*, 763. Hashimoto, T.; Itakura, M.; Shimidzu, N. *J. Chem. Phys.* **1986**, *85*, 6773. Hashimoto, T.; Itakura, M.; Hasegawa, H. *J. Chem. Phys.* **1986**, *85*, 6118.
(18) Okada, M.; Han, C. C. *J. Chem. Phys.* **1986**, *85*, 5317.
(19) Sato, T.; Han, C. C. *J. Chem. Phys.* **1988**, *88*, 2057.
(20) Cahn, J. W.; Hilliard, J. E. *J. Chem. Phys.* **1958**, *28*, 258. Cahn, J. W. *J. Chem. Phys.* **1965**, *42*, 93. Cook, H. E. *Acta Metall.* **1970**, *18*, 297.
(21) Binder, K. *J. Chem. Phys.* **1983**, *79*, 6387.
(22) Furukawa, H. *Prog. Theor. Phys.* **1978**, *59*, 1072. Furukawa, H. *Phys. Rev. Lett.* **1979**, *43*, 136. Furukawa, H. *Physica A* **1984**, *123*, 497.
(23) Siggia, E. D. *Phys. Rev. A* **1979**, *20*, 595.
(24) Stephenson, G. B. *Acta Metall.* **1988**, *36*, 2663. Stephenson, G. B. *J. Non-Cryst. Solids* **1984**, *66*, 393.

(25) Certain commercial materials and equipment are identified in this paper in order to specify adequately the experimental procedure. In no case does such identification imply recommendation or endorsement by the National Institute of Standards and Technology nor does it imply necessarily the best available for the purpose.
(26) Nose, T.; Briber, R. M.; Bauer, B. J., private communication.
(27) Flory, P. J. *Principles of Polymer Chemistry*; Cornell University Press: Ithaca, NY, 1953.
(28) Han, C. C.; Bauer, B. J.; Clark, J. C.; Muraga, Y.; Matsushita, Y.; Okada, M.; Tran-Cong, Q.; Chang, T.; Sanchez, I. C. *Polymer* **1988**, *29*, 2002.
(29) Serman, C. J.; Xu, Y.; Painter, R. C.; Coleman, M. M. *Macromolecules* **1989**, *22*, 2019.
(30) Langer, J. S.; Bar-on, M.; Miller, H. D. *Phys. Rev. A* **1975**, *11*, 1417.
(31) Stephenson, G. B. *Scr. Metall.* **1986**, *20*, 465. Stephenson, G. B.; Warburton, W. K.; Haller, W.; Bienenstock, A. O., private communication.
(32) Hashimoto, T.; Takenaka, M.; Izumitani, T. *Polym. Commun.* **1989**, *30*, 45.
(33) Koningsveld, R.; Onclin, M. H.; Kleintjens, L. A. *Polymer Compatibility and Incompatibility, Principles and Practices*; Šolc, K., Ed.; Harwood Academic for MMI Press: New York, 1980; p 25.

Registry No. HFMS (copolymer), 120721-72-4; poly(butyl methacrylate) (homopolymer), 9003-63-8.